ACS Catalysis

Research Article

Cite This: ACS Catal. 2018, 8, 10581−10589

pubs.acs.org/acscatalysis

Preparation of Cobalt Nanocrystals Supported on Metal Oxides To Study Particle Growth in Fischer−Tropsch Catalysts

Tom W. van Deelen, Jelle J. Nijhuis, Nynke A. Krans, Jovana Zečević, and Krijn P. de Jong*

Inorganic Chemistry and Catalysis, Debye Institute for Nanomaterials Science, Utrecht University, Universiteitsweg 99, 3584 CG Utrecht, The Netherlands

Supporting Information

ABSTRACT: Colloidal synthesis of nanocrystals (NC) followed by their attachment to a support and activation is a promising route to prepare model catalysts for research on structure-performance relationships. Here, we investigated the suitability of this method to prepare well-defined Co/TiO_2 and Co/SiO_2 catalysts for the Fischer−Tropsch (FT) synthesis with high control over the cobalt particle size. To this end, Co-NC of 3, 6, 9, and 12 nm with narrow size distributions were synthesized and attached uniformly on either TiO_2 or SiO_2 supports with comparable morphology and Co loadings of 2−10 wt %. After activation in H_2, the FT activity of the TiO_2-supported 6 and 12 nm Co-NC was similar to that of a Co/TiO_2 catalyst prepared by impregnation, showing that full activation was achieved and relevant catalysts had been obtained; however, 3 nm Co-NC on TiO_2 were less active than anticipated. Analysis after FT revealed that all Co-NC on TiO_2 as well as 3 nm Co-NC on SiO_2 had grown to ∼13 nm, while the sizes of the 6 and 9 nm Co-NC on SiO_2 had remained stable. It was found that the 3 nm Co-NC on TiO_2 already grew to 10 nm during activation in H_2. Furthermore, substantial amounts of Co (up to 60%) migrated from the Co-NC to the support during activation on TiO_2 against only 15% on SiO_2. We showed that the stronger interaction between cobalt and TiO_2 leads to enhanced catalyst restructuring as compared to SiO_2. These findings demonstrate the potential of the NC-based method to produce relevant model catalysts to investigate phenomena that could not be studied using conventionally synthesized catalysts.

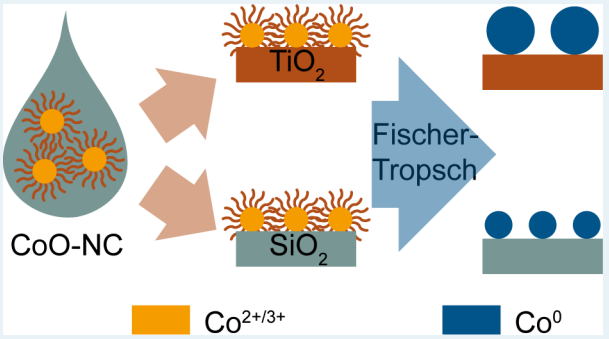

KEYWORDS: *colloidal synthesis, cobalt nanocrystals, supported catalysts, Fischer−Tropsch synthesis, particle growth, metal−support interaction*

INTRODUCTION

Metal nanoparticles on a support material are widely applied as heterogeneous catalysts in industrial processes.[1−4] In order to improve industrial catalyst design, it is a prerequisite to link their structure to their performance which requires well-defined model catalysts.[5,6] Several nanotechnological techniques have recently been developed that allow the synthesis of catalysts with high control over parameters such as composition, size, or shape of metal nanoparticles.[5,7]

Among the available techniques, the colloidal synthesis of nanocrystals (NC) is especially promising for the preparation of catalysts. By preforming the NC in solution instead of directly on the support as is custom in conventional synthesis techniques, it is possible to synthesize monodisperse, single crystalline, and size-controlled NC.[8] The vast majority of the research so far focused on noble metal NC even though base metals are very important for catalysis. However, base metal NC are more challenging to utilize in supported catalysts. First, homogeneous attachment of base metal NC on a support can be hindered by magnetic interactions between the NC.[9] Second, removal of the stabilizing ligand shell can be incomplete, blocking active sites and lowering catalytic activity, or harsh treatments are applied that may compromise the well-defined nature of the catalyst.[10,11] Recently we demonstrated uniform attachment and successful ligand removal for Co-NC supported on carbon nanotubes by applying a mild, low-temperature oxidation to the NC in suspension prior to attachment.[12]

A particular application where NC-based catalysts can contribute to fundamental understanding is the Fischer−Tropsch (FT) synthesis, i.e. the catalytic conversion of synthesis gas (an H_2/CO mixture) into hydrocarbon fuels and chemicals.[13] The cobalt-catalyzed FT reaction is reported to be structure sensitive, related to both cobalt particle size[14,15] and cobalt crystal structure.[16−18] So far, most research involving Co-NC for FT concentrated either on slurry-phase FT, in which the unsupported Co-NC remain in suspension,[19−21] or on Co-NC supported on irreducible oxides (mainly SiO_2 or Al_2O_3).[22−29] However, reducible oxides such

Received: August 3, 2018
Revised: September 25, 2018
Published: October 5, 2018

DOI: 10.1021/acscatal.8b03094
ACS Catal. 2018, 8, 10581−10589

as TiO_2 are also interesting supports for cobalt-based FT catalysts, for both industry[30] and academia.[31]

TiO_2-supported cobalt catalysts can be considered more complex than Co/SiO_2 or Co/Al_2O_3, since TiO_2 can be partially reduced under reaction conditions, leading to special interphase phenomena known as strong metal−support interactions (SMSI).[32,33] The effects of these metal-TiO_2 interactions remain poorly understood, in part because synthesis procedures for well-defined catalysts are lacking, especially for <10 nm Co particles. TiO_2-supported catalysts with narrow Co particle size distributions can be synthesized using conventional methods, but the control over the average particle size is limited.[34,35] Furthermore, there are only a few reports of NC-based Co/TiO_2 catalysts, and these either contained boron impurities owing to the synthesis method[36,37] or the Co-NC were 10 nm or larger.[24,38] Therefore, it would be highly desirable to expand the applicability of Co-NC to TiO_2 as support.

Here we report the synthesis and catalytic performance of well-defined catalysts containing 3−12 nm Co-NC on TiO_2 and SiO_2 and demonstrate their use as model systems by studying particle growth under FT conditions. The Co-NC were synthesized by a hot-injection method. After low-temperature oxidation, the CoO-NC were homogeneously attached to either TiO_2 or SiO_2. Their catalytic performance was comparable to that of Co/TiO_2 prepared by impregnation, except for 3 nm Co-NC on TiO_2, whose activity was substantially lower. The TiO_2-supported Co particles and 3 nm Co-NC on SiO_2 sintered during reduction and/or FT, indicating that both the support and initial NC size affected the stability of Co-NC under reaction conditions. We show that the followed NC-based methodology enabled the synthesis of size-controlled Co/TiO_2 and Co/SiO_2 with relevant catalytic performance. Their potential as model systems is underlined by investigating NC particle growth, revealing phenomena that are not observed with conventionally prepared catalysts.

EXPERIMENTAL METHODS

Cobalt Nanocrystal Synthesis. Cobalt nanocrystals of different sizes were synthesized by a hot injection method based on the literature[39] and our previous work.[12] A schematic summary of the NC synthesis procedure is shown in Figure S1. The benefit of this method is that the required chemicals contain no elements such as phosphorus or boron that might affect the catalyst and its final catalytic performance. The syntheses were performed on a Schlenk line in N_2 atmosphere. In a typical synthesis, 65 mg of oleic acid (Sigma-Aldrich, 90%, technical grade) was degassed under vacuum at 100 °C for 30 min in a 3-necked 100 mL flask with a cooler and two septa. After flushing and switching to N_2, 7.5 mL of 1,2-dichlorobenzene was added under inert atmosphere, and the solution was heated to temperatures between 165 and 182 °C related to the desired NC size. Simultaneously, inside a glovebox, 270 mg of dicobalt octacarbonyl (Acros Organics, 95%, stabilized) was dissolved in 1.5 mL of 1,2-dichlorobenze. This cobalt precursor was then rapidly injected (needle: Ø0.9 × 70 mm) into the heated solution under 750 rpm magnetic stirring and decomposed instantly. The reaction was quenched after 20 min using a water bath. Once at ambient temperature, the N_2 supply was switched off, and one septum was removed to allow low-temperature oxidation by air-exposure under 650 rpm stirring. After 1 h, the mixture was divided over two glass centrifuge tubes, filled to 20 mL with 2-propanol (Sigma-Aldrich, >99%, LC-MS Chromasolv), and centrifuged at 2200 G for 30 min. The supernatant was decanted, and the residue was redispersed in 0.5 mL of *n*-hexane (Acros Organics, 99+ %) per tube by sonication. The tubes were filled to 20 mL with 2-propanol and centrifuged at 2200 G for 40 min. This washing cycle was repeated twice, and after the last step, the residue was redispersed and combined in a total of 2 mL of *n*-hexane.

Cobalt Nanocrystal Attachment. The Co-NC were attached to a support according to the method developed by Casavola et al.[40] A schematic summary of the NC attachment procedure is shown in Figure S1. The supports were TiO_2 (Evonik, Aeroxide P25) or SiO_2 (Evonik, Aerosil OX 50), both sieved to a fraction of 75−150 μm. To regulate the final cobalt loading, between 0.4 and 2.5 g of support was suspended in a mixture of the colloidal suspension and 5−31 mL of 1-octadecene (Sigma-Aldrich, 90%, technical grade) inside a 100 mL 3-necked flask. A cooler, glass plug, and septum were connected to the flask, the magnetic stirring was set to 400 rpm, and the suspension was degassed under vacuum at 100 °C for 15 min, during which the *n*-hexane from the colloidal suspension evaporated. The setup was then flushed, switched to N_2, and heated to 200 °C. The heating was stopped after 30 min at 200 °C, and the solution was cooled to ambient temperature in approximately 30 min. The suspension was divided over two glass centrifuge tubes and centrifuged at 1500 G for 5 min, and the supernatant was decanted. The residue was resuspended in 2 mL of *n*-hexane, sonicated for 1 min, diluted with 6 mL of acetone, and centrifuged at 1500 G for 5 min, and the supernatant was again decanted. This washing cycle was repeated five times, followed by resuspending the residue in 20 mL of acetone, sonicating for 1 min, centrifuging at 1500 G for 5 min, and decanting the supernatant. Afterward, the samples were dried at 60 °C for 1 h in static air, followed by 120 °C for 3 h in static air and 80 °C for 3 h under vacuum. Finally, the samples were sieved to a grain size of 75−150 μm.

Incipient Wetness Impregnation. A comparison Co/TiO_2 sample was prepared by incipient wetness impregnation following the procedure by Eschemann et al.[34] First, 2 g of TiO_2 (Evonik, Aeroxide P25) was sieved to 75−150 μm and then dried at 80 °C for 1 h under vacuum. The vacuum was released and the TiO_2 was impregnated directly afterward with a pore-filling amount of precursor solution consisting of $Co(NO_3)_2{\cdot}6H_2O$ (Acros Organics, 99+ %) in Milli-Q water. The solution was added dropwise under magnetic and manual stirring. After the addition, the powder was dried and heat treated in a U-shaped, glass reactor in fluidized bed mode (1 L·min^{-1} upward flow of N_2). Drying took place at 80 °C for 2 h and was followed directly by a thermal treatment at 250 °C for 2 h, both with 2 °C·min^{-1}. The sample was finally sieved again to a grain size of 75−150 μm.

Plasma Cleaning. Optionally, pristine Co-NC samples were plasma cleaned to remove the ligands prior to reduction and FT. Typically, 100 mg of sample was treated for 8 h in a homemade container inserted into a Fischione Model 1020 Plasma Cleaner. The plasma was generated using a 25% O_2 in Ar flow and a 13.56 MHz oscillating electromagnetic field.

Characterization. Transmission electron microscopy (TEM) was performed either on a Tecnai 12 (FEI), operated at 120 kV, or on a Tecnai 20 (FEI), operated at 200 kV. TEM samples of Co-NC suspensions were prepared by sonicating and dropcasting a diluted sample directly on a carbon-coated TEM grid. To prepare a sample of supported Co-NC, the solid

DOI: 10.1021/acscatal.8b03094
ACS Catal. 2018, 8, 10581−10589

was first suspended in 2-propanol by sonication and then dropcasted on a TEM grid. In the case of samples after catalysis, the samples were washed three times using toluene and 30 min sonication and once using *n*-hexane to remove the hydrocarbon reaction products before dropcasting on a TEM grid. The sizes of >200 Co particles were determined manually using ImageJ software. All particle sizes are reported as the Sauter mean diameter (volume/surface mean, D[3,2]) of the equivalent metallic cobalt particles, meaning that the measured diameters of (partial) cobalt oxide particles were corrected based on the densities of the oxide and the metal.

Scanning transmission electron microscopy combined with energy-dispersive X-ray spectroscopy (STEM-EDX) was performed in high-angle annular dark-field (HAADF) mode on a Talos F200X (FEI), equipped with a high-brightness field emission gun (X-FEG) and a Super-X G2 EDX detector and operated at 200 kV. Particle size analysis was similar to that of TEM, with the exception that <200 particles were analyzed for some samples, depending on the particle size and cobalt loading.

HAADF-STEM-EDX of the same positions of 12 nm Co-NC on TiO_2 before and after reduction was performed using a SiN TEM chip (TEMWindow SN100-A50Q33). After imaging the pristine sample, the SiN TEM chip was transferred to a glass U-shaped reactor, and the sample on the chip was reduced *ex situ* in 25% H_2 in Ar flow at 350 °C for 8 h with 1 °C·min^{-1} and cooled down afterward under the same atmosphere. Subsequently, the chip was transferred back to the microscope and analyzed again. During the transfer, the sample was exposed to air at ambient conditions.

N_2-physisorption of the bare supports was measured at −196 °C on a Tristar 3000 (Micromeritics). The samples were dried in N_2 at 300 °C for 14−20 h prior to the analysis.

Inductively coupled plasma-optical emission spectroscopy (ICP-OES) was carried out on a SPECTRO ARCOS, and the sample was digested in aqua regia to extract the cobalt.

Temperature programed reduction (TPR) profiles were measured on an Autochem 2920 (Micromeritics). Approximately 100 mg of sample was reduced in 5% H_2 in Ar flow from 50 to 800 °C with 5 °C·min^{-1}.

X-ray diffraction (XRD) was performed on a Bruker D2 Phaser, equipped with a Co radiation source (λ = 1.789 Å). The sample was measured between 20 and 100° 2θ with an increment of 0.05°.

Fischer−Tropsch Synthesis. The catalytic performance in the Fischer−Tropsch synthesis was investigated using an Avantium Flowrence 16 parallel reactor setup. Stainless steel plug flow reactors of 2.0 or 2.6 mm ID were loaded with 25−110 mg of catalyst (75−150 μm) diluted with 100 mg of SiC (200−425 μm). Prior to reaction, the catalysts were reduced *in situ* at 1 bar in 25% H_2 in He flow at either 350 °C (TiO_2-samples) or 500 °C (SiO_2-samples) for 8 h with 1 °C·min^{-1}. Afterward, the reactors were cooled to 180 °C and pressurized to 20 bar. At these conditions, the atmosphere was switched to synthesis gas with H_2/CO = 2 (v/v) and 5% He as internal standard. Subsequently, the reactors were heated to 220 °C with 1 °C·min^{-1}, and product analysis was started after 1 h. The reaction products were analyzed online using an Agilent 7890A GC equipped with two channels. The first channel contained an Agilent J&W PoraBOND Q column connected to an FID to detect the hydrocarbon products, and the second one consisted of a ShinCarbon-ST column connected to a TCD to analyze the permanent gases.

The catalytic activity was reported as CO conversion (X_{CO}), cobalt time yield (CTY), and turnover frequency (TOF). The TOF was based on the activity and the Sauter mean diameter (D[3,2]) of the spent Co-NC after correction for a 3 nm CoO passivation layer, assuming a cross-sectional area of 0.0662 nm^2 per cobalt atom.[41] The selectivity (%$_C$) to C_1−C_4 products was defined as S_{C1-C4} = 100 %·F_{Cn}·n·($F_{CO,in}$·X_{CO})$^{-1}$ with n being the product's carbon number and F being the flow of the corresponding hydrocarbon or CO. The selectivity to C_{5+} was defined as S_{C5+} = 100 % − S_{C1-C4}.

RESULTS AND DISCUSSION

Cobalt Nanocrystal Synthesis. Well-defined cobalt nanocrystals were synthesized with distinct sizes between 3 and 12 nm and a polydispersity of 11−18% (Figure 1, additional particle size distributions in Figure S2). The Co-NC were designated as CoX, with X denoting the average diameter of the NC. The size of the Co-NC size was regulated by varying the temperature of the hot injection synthesis, which is in line with the literature.[39,42] The Co-NC size correlated with the synthesis temperature in the range of 170−183 °C and

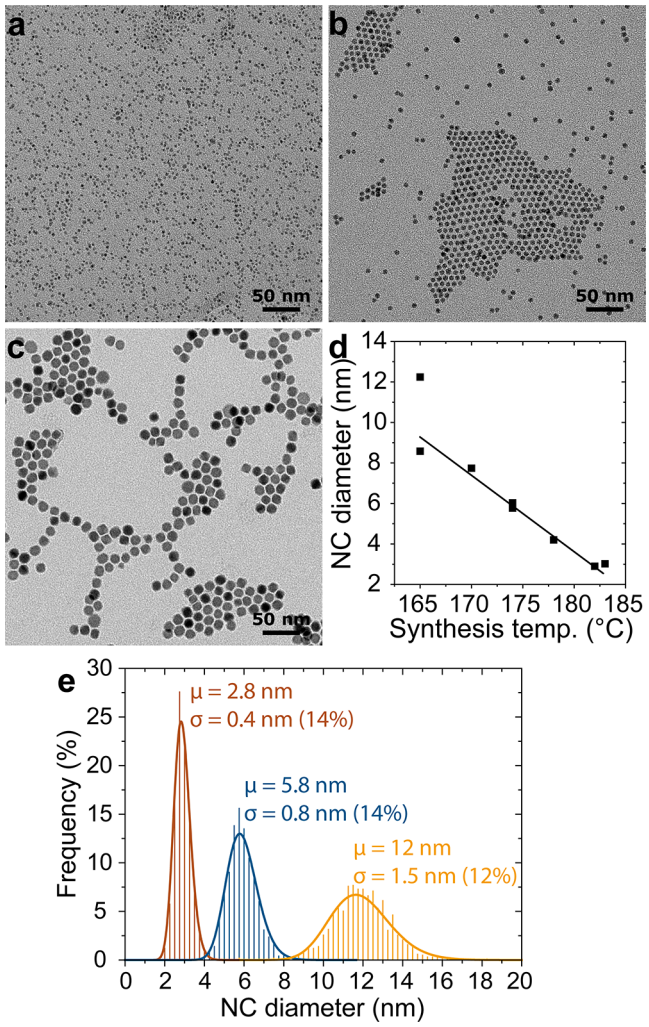

Figure 1. Overview of the as-synthesized Co-NC. TEM images of (a) Co3, (b) Co6, and (c) Co12 and (d) the resulting Co-NC size as a function of the hot-injection temperature. (e) Histograms and the log-normal distributions of selected sizes of Co-NC.

DOI: 10.1021/acscatal.8b03094
ACS Catal. 2018, 8, 10581−10589

became less reproducible at lower temperature (Figure 1d). After the synthesis, low-temperature oxidation by air-exposure at ambient conditions was applied to facilitate attachment and activation of the Co-NC.[12] The Co-NC of 3, 6, 9, and 12 nm were attached to TiO_2 or SiO_2, thus omitting the Co-NC of 4 and 8 nm in Figure 1d.

Cobalt Nanocrystal Attachment. The Co-NC were attached to titania and silica with comparable specific surface areas (~50 $m^2 \cdot g^{-1}$) but different mesopore volumes (0.3 and 0.1 $mL \cdot g^{-1}$, respectively) as determined by N_2-physisorption (Figure S3, Table S1). The cobalt loading was adjusted to obtain similar cobalt metal surface areas per unit weight of catalyst in the pristine samples with the aim to avoid major differences in catalyst-weight-based activities during FT (Table 1). Furthermore, the Co-NC on the supports were analyzed with TEM (Figure 2). The Co-NC distribution was uniform over both supports, similar to previous results with a carbon support.[12,40] In addition, a reference Co/TiO_2 sample was prepared by conventional techniques, in this case incipient wetness impregnation of a cobalt nitrate solution (designated as IWI-Co/TiO_2, details in Table 1 and TEM results in Figure S4). Its average particle size was most comparable to $Co6/TiO_2$, but the particle size distribution was substantially broader.

Table 1. Characteristics of the Supported Co-NC and IWI-Co Samples[a]

sample	$D[3,2]_{Co\text{-}NC}$ (nm)	Co loading (wt %)	initial Co surface area ($m_{Co}^2 \cdot g_{Cat}^{-1}$)
$Co3/TiO_2$	2.9 ± 0.4	2.4	5.7
$Co6/TiO_2$	6.0 ± 0.8	4.6	5.5
$Co12/TiO_2$	12 ± 1.5	8.7	5.4
IWI-Co/TiO_2	7.3 ± 2.5	6.7	6.2
$Co3/SiO_2$	2.8 ± 0.5	3.6	6.8
$Co6/SiO_2$	5.6 ± 0.6	6.8	9.2
$Co9/SiO_2$	8.6 ± 1.1	9.6	7.7

[a]The Sauter mean diameter (± standard deviation) of the Co-NC was analyzed by TEM before attachment and recalculated to the corresponding Co^0 particle sizes. The Co loading was determined by ICP-OES. Based on these two results, a Co specific surface area of the pristine catalysts was calculated.

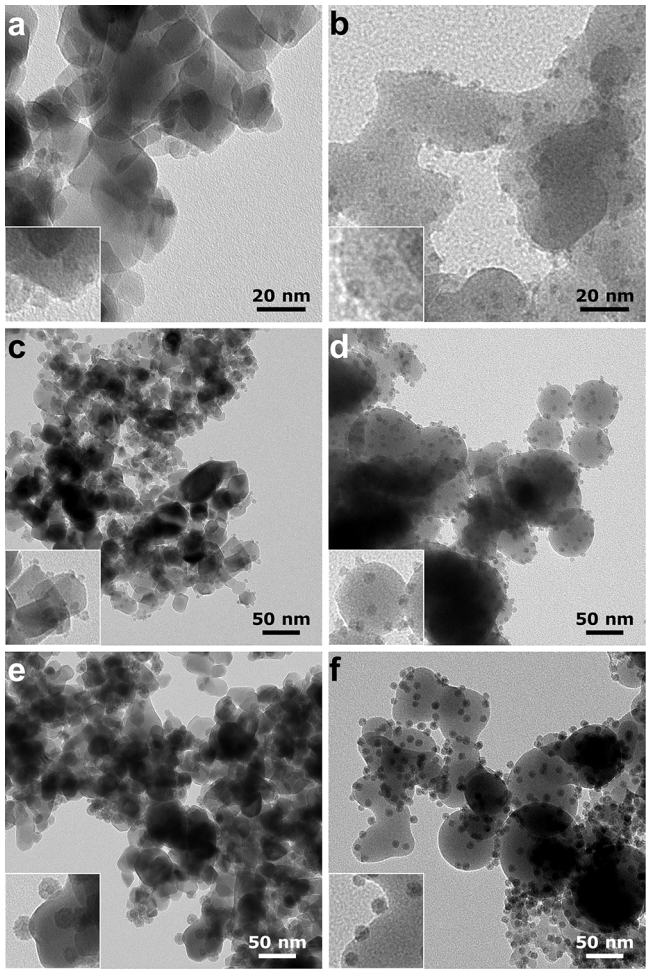

Figure 2. Overview of the Co-NC attached to a support. The TiO_2-supported samples are in the left column, and the SiO_2-supported samples are in the right column. (a) $Co3/TiO_2$, (b) $Co3/SiO_2$, (c) $Co6/TiO_2$, (d) $Co6/SiO_2$, (e) $Co12/TiO_2$, and (f) $Co9/SiO_2$. The insets are at double the magnification of the original image.

The sizes of the Co-NC remained unchanged during the attachment treatment as concluded from TEM (Figure 2). The Co-NC of 3 and 6 nm consisted completely of CoO,[12] while for the 9 and 12 nm Co-NC only an outer layer of CoO was formed and a metallic core with higher contrast was observed. This CoO shell had a thickness of 4.5 nm in the case of $Co12/TiO_2$, which exceeds the CoO passivation layer of 3 nm that is typically observed upon exposure of metallic cobalt particles to air at ambient conditions.[43] The increased oxidation of the Co-NCs could have occurred during drying at 120 °C, as this is close to the temperature range where Kirkendall effects have been observed.[44] The Kirkendall effect occurs upon oxidation of metals at elevated temperatures and leads to the formation of hollow metal oxide particles.[11,45]

The reducibility of the Co-NC on TiO_2 samples was investigated by temperature-programmed reduction (TPR, Figure 3a). Two reduction peaks were observed between 250 and 450 °C for all samples next to a negative peak at higher temperatures, which is attributed to the desorption/decomposition of remaining ligands.[12] As expected, the reduction shifted to lower temperatures with increasing particle size, because small oxide particles often display lower reducibility.[46−48] Furthermore, the total H_2-uptake related to the first two peaks increased with the particle size following the increase in cobalt content. When comparing the total H_2-uptake of the Co-NC/TiO_2 samples normalized to the amount of Co, the H_2-uptake of $Co12/TiO_2$ was only 89−92% of that of the 3 and 6 nm NC (deconvolutions in Figure S5). This indicated that ~10% of the cobalt in $Co12/TiO_2$ was still present in the core of the NC as metallic cobalt, which was in line with the earlier TEM observation of a metallic core and a CoO passivation layer (Figure 2).

Fischer−Tropsch Synthesis. The cobalt-weight-based activity (cobalt time yield, CTY) of the TiO_2-supported samples was evaluated over 100 h on stream (Figure 3b, Table 2). $Co6/TiO_2$ was the most active after 100 h followed by $Co12/TiO_2$, which was initially more active but deactivated faster. $Co3/TiO_2$ was a factor 5 less active per unit weight of cobalt over the entire time range studied. Interestingly, the 6 and 12 nm Co-NC catalysts were similar or even higher in CTY than the IWI-Co/TiO_2 catalyst, indicating that these Co-NC were adequately activated and that relevant catalytic results were obtained with these NC-based model systems.

DOI: 10.1021/acscatal.8b03094
ACS Catal. 2018, 8, 10581−10589

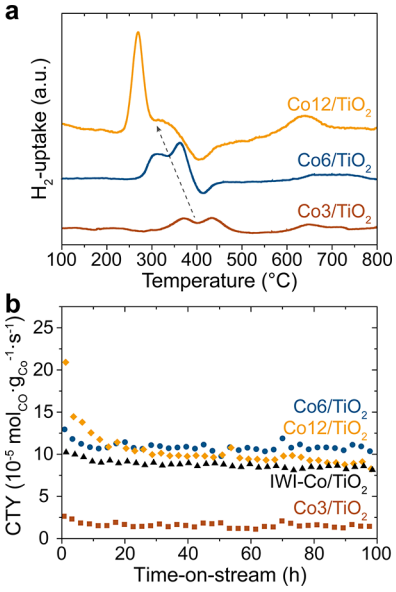

Figure 3. Reduction and catalytic activity of the TiO_2-supported samples. (a) Reduction profiles obtained by TPR normalized to the mass of sample and (b) catalytic activity (CTY) in FT as a function of time-on-stream at 20 bar, 220 °C, 2 H_2/CO (v/v), GHSV = 1950−5900 h^{-1}, and X_{CO} = 5−60%.

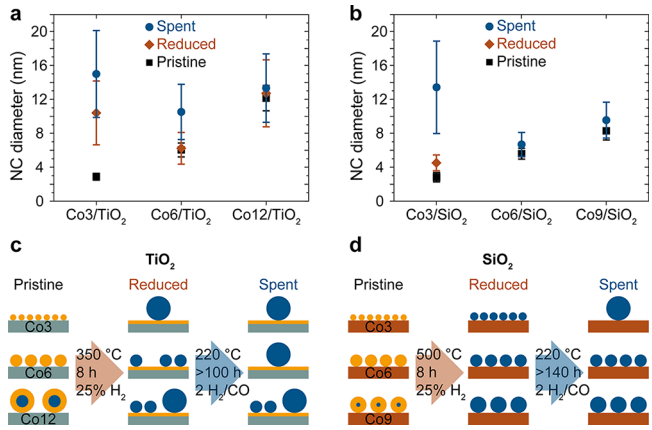

Figure 4. Average cobalt particle sizes of the samples in the pristine, reduced, and spent state. (a,b) Average Co-NC sizes from TEM analysis of the TiO_2- and SiO_2-supported samples, respectively. The bars give the standard deviation of the average particle size. Schematic illustration of the sintering behavior of the different sizes on (c) TiO_2 and on (d) SiO_2 after different treatments. In these illustrations, Co^{2+} or Co^{3+} is depicted in yellow, and Co^0 is depicted in blue. Migration of Co to TiO_2 during reduction was observed by EDX.

Furthermore, the selectivity toward C_{5+} products was around 85% for all TiO_2-supported samples, except for Co3/TiO_2 whose C_{5+}-selectivity was only 57% (Table 2).

The catalytic activity of the Co/SiO_2 samples was investigated over 100 h on stream at CO conversion levels between 15 and 30% (Figure S6, Table 2). The cobalt-weight-based activities of Co6/SiO_2 and Co9/SiO_2 were the highest of all investigated catalysts. The 3 nm Co-NC displayed again the lowest activity of the series, yet Co3/SiO_2 was a factor 6 more active per unit weight of cobalt than Co3/TiO_2. The C_{5+}-selectivities of the SiO_2-supported catalysts varied between 76 and 79% and were overall lower than that of most TiO_2-supported catalysts (~85%). This observation corresponds well with earlier findings of TiO_2 promoting the C_{5+}-selectivity of cobalt catalysts in FT.[49]

The deactivation and observed differences in activity could be caused by several mechanisms, such as carbon deposition,[50] metal−support compound formation,[51] or net particle growth.[51] To investigate the occurrence of particle growth in more detail, the spent catalysts were analyzed with TEM (Table 2, Figure 4, Figure S7). All Co-NC supported on TiO_2, as well as the IWI-Co/TiO_2, had grown to ~13 nm on average, which was in line with recently reported particle sizes of a Co−Re/TiO_2 catalyst after various periods on stream.[51] On SiO_2, the initially 3 nm Co-NC had also sintered to 13 nm, while the 6 and 9 nm Co-NC were stable.

Using the particle sizes of the spent catalysts and the activities at 90−100 h on stream, the surface-specific activities (turnover frequencies, TOF) were calculated (Table 2). The TOF of all TiO_2-supported catalysts except Co3/TiO_2 was around 65 × 10^{-3} s^{-1}, in line with previous reports.[52−54] The identical TOF of 6 and 12 nm Co-NC on TiO_2 and the IWI-Co/TiO_2 catalyst showed that the active cobalt sites were not affected by the presence of residual ligands or other factors specific to the NC-based synthesis method. The apparent TOF of Co3/TiO_2, based on the particle size of the catalyst and the end-of-run activity, was only 12 × 10^{-3} s^{-1} (Table 2). This was remarkable, because the Co particles in Co3/TiO_2 had grown outside of the size regime where particle size effects typically cause low activities (<6−8 nm).[14,15,22] Therefore, a TOF similar to the others (65 × 10^{-3} s^{-1}) should have been obtained. Instead, the low apparent TOF was ascribed to loss of cobalt from the metal particles to the TiO_2 resulting in less metallic surface area available for catalysis. Judging from the decrease in TOF, up to 80% of the cobalt was lost in this manner.

Table 2. Catalytic Performance at 20 bar, 220 °C, and 2 H_2/CO (v/v)[b]

sample	GHSV (h^{-1})	X_{CO} (%)	CTY[a]	TOF (10^{-3} s^{-1})	S_{C1} (%C)	S_{C2-C4} (%C)	S_{C5+} (%C)	D[3,2]$_{spent}$ (nm)
Co3/TiO_2	2000	4.6	1.4	12	21	21	57	15 ± 5.1
Co6/TiO_2	3100	23	11	66	9.2	8.1	83	11 ± 3.3
Co12/TiO_2	6900	24	8.6	68	8.2	5.9	86	13 ± 4.0
IWI-Co/TiO_2	7500	18	8.4	68	8.7	7.0	84	14 ± 5.9
Co3/SiO_2	1500	25	8.5	67	13	12	76	13 ± 5.5
Co6/SiO_2	5500	16	21	82	14	11	76	6.7 ± 1.4
Co9/SiO_2	10800	21	19	106	13	8.7	79	9.6 ± 2.1

[a]in 10^{-5} $mol_{CO}·g_{Co}^{-1}·s^{-1}$. [b]The reported data was obtained after 90−100 h on stream. The TOF was based on the end-of-run activity and Co particle size (D[3,2]) of the spent samples. The Sauter mean diameter (± standard deviation) of the Co-NC was analyzed in the spent and passivated state and corrected for the lattice expansion due to the 3 nm CoO passivation layer.

DOI: 10.1021/acscatal.8b03094
ACS Catal. 2018, 8, 10581−10589

The TOF of the SiO_2-supported catalysts increased with initial particle size (Table 2). In the case of the initially 3 nm Co-NC on SiO_2, the TOF was 67 × 10^{-3} s^{-1}, which was similar to most Co/TiO_2 catalysts and already somewhat higher than previously reported for Co/SiO_2 catalysts.[55] However, the intrinsic activities of 6 and 9 nm Co-NC on SiO_2 were exceptionally high in comparison to the literature. A possible explanation for the different TOF of Co-NC and conventional catalysts could be that the Co-NC approach led to cobalt particles with a higher fraction of *hcp* Co, which is more active in FT than *fcc* Co.[16−18,56] Alternatively, the Co-NC could have less interaction with the support, because the Co-NC were formed prior to attachment to the support. For example, when comparing the TEM results of spent Co/SiO_2, the grown particles of $Co3/SiO_2$ were mainly confined between primary SiO_2 particles where the contact area with the support was maximal (Figure S7). The Co-NC in $Co6/SiO_2$ and $Co9/SiO_2$, on the other hand, were still distributed uniformly over the support, and as such, a higher fraction of the cobalt surface area would be accessible to reactants.

Overall, the employed NC-based approach to catalyst synthesis yielded well-defined model systems with reasonable control over the initial NC size and relevant catalytic performance. It is therefore anticipated that these model catalysts are suitable to investigate structure-performance relationships, and already some interesting phenomena were observed here, especially on the growth of NC of specific sizes under reaction conditions. These observations will be investigated and discussed in more detail in the next section.

Sintering of Cobalt Nanocrystals. To investigate the growth of Co-NC, the particle sizes were analyzed using TEM after reduction as well as after catalysis (Figure 4). The 3 nm Co-NC on TiO_2 sintered to particles of 10 nm already during reduction and grew further to 15 nm during FT. The 3 nm Co-NC on SiO_2 ultimately grew to the same extent, but in this case the particles predominantly sintered during FT. The reduction barely affected the particle size of $Co3/SiO_2$ even though the reduction was performed at 500 °C.

EDX maps of the reduced and passivated TiO_2-supported catalysts and $Co3/SiO_2$ were quantified to investigate the location of Co on the supports (Table 3, see Figure S8 for results and experimental details). Compared to ICP (Table 1), the total cobalt loading from EDX was 30−50% higher on TiO_2 and 50% lower on SiO_2. Therefore, relative differences for one and the same sample were considered more representative than the absolute values.

Table 3. Quantification of the Cobalt Present in the Support and in Particles after Reduction of Co/TiO_2 and $Co3/SiO_2$[a]

sample	Co_{total} (wt %)	$Co_{particles}$ (wt %)	$Co_{support}$ (wt %)	$Co_{particles}/Co_{total}$	$Co_{support}/Co_{total}$
$Co3/TiO_2$	3.3	1.3	2.0	0.38	0.62
$Co6/TiO_2$	6.8	4.1	2.7	0.61	0.39
$Co12/TiO_2$	11	9.2	2.2	0.81	0.19
$Co3/SiO_2$	2.4	2.0	0.4	0.84	0.16

[a]The total Co loading and the fractions of Co in particles and Co in the support were derived from HAADF-STEM-EDX (Figure S8).

For the reduced and passivated Co/TiO_2 samples, ∼2.5 wt % of Co was found dispersed in the support and not in particles, regardless of NC size and loading. In the case of $Co3/TiO_2$, this amounted to approximately 60% of the total cobalt content from EDX and might be partially responsible for its low CTY. Furthermore, the Co signal in the EDX maps occasionally followed the contours of TiO_2 particles with increased intensity at the surface (Figure S8). This means that a higher Co concentration existed at the surface than in the bulk of the TiO_2 particles. In contrast, only 16% of the Co was found on the silica support for $Co3/SiO_2$, and the remaining 84% was still present in Co particles. Consequently, no contours of the support were observed in the Co signal from EDX at locations without any particles (Figure S8). These EDX results show that, during reduction, cobalt migrated to the support more with TiO_2 than with SiO_2, as illustrated in Figure 4c,d. These cobalt species on the support were not detected in XRD (Figure S9), probably because of their low concentration and/or low crystallinity. Additionally, the amount of cobalt on the support was assumed to remain constant during FT, because the Co/TiO_2 catalysts did not activate, which would be expected if the cobalt species on the support were reduced under reaction conditions (Figure 3b).

Small particles have a higher thermodynamic potential[57] and are therefore more prone to sintering.[58,59] Interestingly, in these earlier studies, growth took place via monomers that were created upon exposure to CO under reaction conditions. For example, in the case of Co/Al_2O_3, cobalt subcarbonyls were proposed as monomers that migrate over the support and give rise to particle growth via Ostwald ripening.[60−62] However, in our $Co3/TiO_2$ sample, a large part of the growth took place already during reduction, so sintering was not induced by CO. When combining these results with the tendency of 60% of the cobalt in the NC to "leach" to the surface of the TiO_2, we propose that different mobile species, possibly cobalt titanates,[63] spread out over the support and cause a few particles to grow large. This hypothesis is in line with thermodynamic calculations (Figure S10), which showed that it is thermodynamically possible to form small amounts of cobalt titanates under reduction conditions, and agrees with previous observations.[64−66] Notably, Cats et al.[64] observed a thin layer of Co species surrounding TiO_2 particles, albeit in spent and not in reduced catalysts.

On SiO_2, the formation of cobalt silicates during reduction is thermodynamically limited (Figure S10), and the growth of 3 nm Co-NC occurred mainly during FT. The sintering might therefore be ascribed to CO-induced Ostwald ripening as observed before by Kistamurthy et al.[67] or particle migration and coalescence. Furthermore, 8 h plasma cleaning of the pristine samples to remove ligands reduced the particle growth for $Co3/SiO_2$ but not for $Co3/TiO_2$ (Figure S11). This further confirmed that the mechanism responsible for particle growth is different on both supports even though the final particle size is similar.

The 6 nm Co-NC on TiO_2 did not grow during reduction (Figure 4). The driving force for sintering during reduction was thus less than for $Co3/TiO_2$ because of the larger particle size. However, the NC on TiO_2 did grow to 11 nm during FT. Growth of the 6 nm Co-NC was not observed on SiO_2 even after catalysis, showing that the Co-NC are less stable on TiO_2 compared to SiO_2. Interestingly, $Co6/TiO_2$ had sintered less than IWI-Co/TiO_2 after FT, with final particles sizes of 11 and 14 nm, respectively (Figure S12). Because the average particle

DOI: 10.1021/acscatal.8b03094
ACS Catal. 2018, 8, 10581−10589

sizes of both samples were initially comparable while the polydispersity of IWI-Co/TiO_2 was higher, this shows the impact of the width of the particle size distribution on the stability of the cobalt nanoparticles.[68−70] It nicely illustrates the advantage of the NC-based approach over the traditional synthesis techniques to arrive at more stable catalysts.

On average, 12 nm Co-NC on TiO_2 did not grow, but the particle size distribution did become broader already after reduction (Figure 4). Both smaller and larger particles were thus formed, which implied Ostwald ripening or redispersion of cobalt, possibly via cobalt-ion migration, under reducing conditions. No evidence of Co-NC growth or redispersion was apparent on Co9/SiO_2 indicating that Co mobility was more extensive with the TiO_2 support or the somewhat larger Co-NC sizes. Extending the reduction to 16 h instead of 8 h did not change the particle size distribution of Co12/TiO_2 further (Figure S13). This observation is qualitatively in line with the results of Xaba et al.[71] on titania P25, although their Co particles were substantially larger (~50 nm).

The size evolution of individual Co-NC in Co12/TiO_2 was followed before and after reduction and passivation to investigate the redispersion in more detail (Figure 5). No

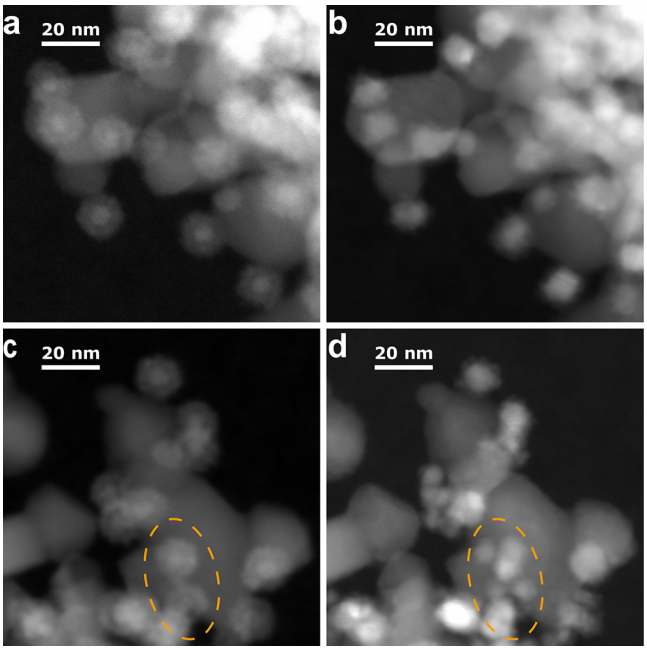

Figure 5. Size evolution of individual Co-NC in Co12/TiO_2 during reduction. (a,c) HAADF-STEM images of pristine Co12/TiO_2 and (b,d) HAADF-STEM images of the same locations after reduction at 350 °C for 8 h. The highlighted area contains two particles that disintegrated during reduction and formed multiple smaller particles.

particles were found that had moved from their original position, indicating low mobility of the Co-NC as a whole and making migration and coalescence unlikely as a pathway for particle growth during reduction. Furthermore, approximately 5% of the particles broke up into multiple smaller particles (Figure 5c,d highlighted area, Figure S14). This redispersion caused an increase in the fraction of 5−8 nm particles, resulting in broadening of the particle size distribution.

Two reasons can be proposed for the disintegration of the NC. First, it might be favorable for certain particles to maximize their contact area with the support, since the interaction between metals and reducible supports such as TiO_2 can lead to dynamic systems under reducing conditions.[44] Second, the core−shell structure in pristine Co12/TiO_2 could be an intermediate stage of the Kirkendall effect.[11] Sasdavian et al.[45] investigated this effect for Co-NC of different sizes on SiO_2 and reported similar core−shell particles in the case of incomplete oxidation of 29 nm particles. Completely oxidized, hollow cobalt oxide particles of 29 nm disintegrated into multiple smaller particles upon reduction, whereas smaller hollow particles returned to their original size of 11 nm. Based on these results, our 12 nm Co-NC, being similar in size to their 11 nm particles, are not expected to disintegrate upon reduction.

CONCLUSIONS

Here, we investigated the preparation of well-defined TiO_2- and SiO_2-supported catalysts via colloidal synthesis of Co-NC and evaluated their catalytic performance in the Fischer−Tropsch synthesis. The 3−12 nm Co-NC were synthesized by a hot-injection method, oxidized at low temperature to restrict magnetic interactions and subsequently attached to TiO_2 or SiO_2. The catalytic activity of most TiO_2-supported samples was in line with that of a Co/TiO_2 sample prepared by impregnation of cobalt nitrate, proving that relevant catalytic data was obtained with these model catalysts. The cobalt-weight-based activity of 3 nm Co-NC on TiO_2 was 5-fold lower than expected, and this was partially ascribed to loss of cobalt to the support. Furthermore, the TiO_2-supported Co particles and 3 nm Co-NC on SiO_2 sintered, while 6 and 9 nm Co-NC on SiO_2 were stable during reduction and FT. We showed that the interaction between Co(O) and TiO_2 was responsible for the decreased stability of the Co-NC. This study illustrates the promise of synthesizing model catalysts using colloidal techniques, as the high precision in particle size enabled the investigation of effects that have not have been revealed earlier with conventional synthesis techniques.

ASSOCIATED CONTENT

Supporting Information

The Supporting Information is available free of charge on the ACS Publications website at DOI: 10.1021/acscatal.8b03094.

Schematic summary of the catalyst synthesis procedure, additional characterization, and catalytic results (PDF)

AUTHOR INFORMATION

Corresponding Author

*E-mail: k.p.dejong@uu.nl.

ORCID

Tom W. van Deelen: 0000-0002-3666-4576

Notes

The authors declare no competing financial interest.

ACKNOWLEDGMENTS

T.W.v.D and K.P.d.J. acknowledge Shell Global Solutions and The Netherlands Association for Scientific Research (NWO) for funding through the CHIPP framework. N.A.K., J.Z., and K.P.d.J. acknowledge the European Research Council, EU FP7 ERC Advanced Grant no. 338846 for funding. We thank Pasi Paalanen and Lennart Weber (N_2-physisorption), Carlos Hernández Mejía (TPR), and Helen de Waard (ICP-OES) for the measurements indicated.

DOI: 10.1021/acscatal.8b03094
ACS Catal. 2018, 8, 10581−10589

REFERENCES

(1) Zečević, J.; Vanbutsele, G.; de Jong, K. P.; Martens, J. A. Nanoscale Intimacy in Bifunctional Catalysts for Selective Conversion of Hydrocarbons. *Nature* **2015**, *528*, 245−248.

(2) Behrens, M.; Studt, F.; Kasatkin, I.; Kühl, S.; Hävecker, M.; Abild-pedersen, F.; Zander, S.; Girgsdies, F.; Kurr, P.; Kniep, B.-L.; Tovar, M.; Fischer, R. W.; Nørskov, J. K.; Schlögl, R. The Active Site of Methanol Synthesis over $Cu/ZnO/Al_2O_3$ Industrial Catalysts. *Science* **2012**, *336*, 893−898.

(3) Cargnello, M.; Doan-Nguyen, V. V. T.; Gordon, T. R.; Diaz, R. E.; Stach, E. A.; Gorte, R. J.; Fornasiero, P.; Murray, C. B. Control of Metal Nanocrystal Size Reveals Metal-Support Interface Role for Ceria Catalysts. *Science* **2013**, *341*, 771−773.

(4) Torres Galvis, H. M.; Bitter, J. H.; Khare, C. B.; Ruitenbeek, M.; Dugulan, A. I.; de Jong, K. P. Supported Iron Nanoparticles as Catalysts for Sustainable Production of Lower Olefins. *Science* **2012**, *335*, 835−838.

(5) Zaera, F. Nanostructured Materials for Applications in Heterogeneous Catalysis. *Chem. Soc. Rev.* **2013**, *42*, 2746−2762.

(6) Jia, C.-J.; Schüth, F. Colloidal Metal Nanoparticles as a Component of Designed Catalyst. *Phys. Chem. Chem. Phys.* **2011**, *13*, 2457−2487.

(7) Munnik, P.; de Jongh, P. E.; de Jong, K. P. Recent Developments in the Synthesis of Supported Catalysts. *Chem. Rev.* **2015**, *115*, 6687−6718.

(8) An, K.; Somorjai, G. A. Size and Shape Control of Metal Nanoparticles for Reaction Selectivity in Catalysis. *ChemCatChem* **2012**, *4*, 1512−1524.

(9) Werner, S.; Johnson, G. R.; Bell, A. T. Synthesis and Characterization of Supported Cobalt-Manganese Nanoparticles as Model Catalysts for Fischer−Tropsch Synthesis. *ChemCatChem* **2014**, *6*, 2881−2888.

(10) Zacharaki, E.; Beato, P.; Tiruvalam, R. R.; Andersson, K. J.; Fjellvåg, H.; Sjåstad, A. O. From Colloidal Monodisperse Nickel Nanoparticles to Well-Defined Ni/Al_2O_3 Model Catalysts. *Langmuir* **2017**, *33*, 9836−9843.

(11) Yin, Y.; Rioux, R. M.; Erdonmez, C. K.; Hughes, S.; Somorjai, G. A.; Alivisatos, A. P. Formation of Hollow Nanocrystals Through the Nanoscale Kirkendall Effect. *Science* **2004**, *304*, 711−714.

(12) van Deelen, T. W.; Su, H.; Sommerdijk, N. A. J. M.; de Jong, K. P. Assembly and Activation of Supported Cobalt Nanocrystal Catalysts for the Fischer−Tropsch Synthesis. *Chem. Commun.* **2018**, *54*, 2530−2533.

(13) Zhong, L.; Yu, F.; An, Y.; Zhao, Y.; Sun, Y.; Li, Z.; Lin, T.; Lin, Y.; Qi, X.; Dai, Y.; Gu, L.; Hu, J.; Jin, S.; Shen, Q.; Wang, H. Cobalt Carbide Nanoprisms for Direct Production of Lower Olefins from Syngas. *Nature* **2016**, *538*, 84−87.

(14) Bezemer, G. L.; Bitter, J. H.; Kuipers, H. P. C. E.; Oosterbeek, H.; Holewijn, J. E.; Xu, X.; Kapteijn, F.; van Dillen, A. J.; de Jong, K. P. Cobalt Particle Size Effects in the Fischer−Tropsch Reaction Studied with Carbon Nanofiber Supported Catalysts. *J. Am. Chem. Soc.* **2006**, *128*, 3956−3964.

(15) den Breejen, J. P.; Radstake, P. B.; Bezemer, G. L.; Bitter, J. H.; Frøseth, V.; Holmen, A.; de Jong, K. P. On the Origin of the Cobalt Particle Size Effects in Fischer−Tropsch Catalysis. *J. Am. Chem. Soc.* **2009**, *131*, 7197−7203.

(16) Sadeqzadeh, M.; Karaca, H.; Safonova, O. V.; Fongarland, P.; Chambrey, S.; Roussel, P.; Griboval-Constant, A.; Lacroix, M.; Curulla-Ferré, D.; Luck, F.; Khodakov, A. Y. Identification of the Active Species in the Working Alumina-Supported Cobalt Catalyst under Various Conditions of Fischer−Tropsch Synthesis. *Catal. Today* **2011**, *164*, 62−67.

(17) Liu, J.-X.; Su, H.-Y.; Sun, D.-P.; Zhang, B.-Y.; Li, W.-X. Crystallographic Dependence of CO Activation on Cobalt Catalysts: HCP versus FCC. *J. Am. Chem. Soc.* **2013**, *135*, 16284−16287.

(18) Lyu, S.; Wang, L.; Zhang, J.; Liu, C.; Sun, J.; Peng, B.; Wang, Y.; Rappé, K. G.; Zhang, Y.; Li, J.; Nie, L. Role of Active Phase in Fischer−Tropsch Synthesis: Experimental Evidence of CO Activation over Single-Phase Cobalt Catalysts. *ACS Catal.* **2018**, *8*, 7787−7798.

(19) Gual, A.; Godard, C.; Castillón, S.; Curulla-Ferré, D.; Claver, C. Colloidal Ru, Co and Fe-Nanoparticles. Synthesis and Application as Nanocatalysts in the Fischer−Tropsch Process. *Catal. Today* **2012**, *183*, 154−171.

(20) Wang, H.; Zhou, W.; Liu, J.-X.; Si, R.; Sun, G.; Zhong, M.-Q.; Su, H.-Y.; Zhao, H.-B.; Rodriguez, J. A.; Pennycook, S. J.; Idrobo, J.-C.; Li, W.-X.; Kou, Y.; Ma, D. Platinum-Modulated Cobalt Nanocatalysts for Low-Temperature Aqueous-Phase Fischer−Tropsch Synthesis. *J. Am. Chem. Soc.* **2013**, *135*, 4149−4158.

(21) Delgado, J. A.; Claver, C.; Castillón, S.; Curulla-Ferré, D.; Godard, C. Correlation between Hydrocarbon Product Distribution and Solvent Composition in the Fischer−Tropsch Synthesis Catalyzed by Colloidal Cobalt Nanoparticles. *ACS Catal.* **2015**, *5*, 4568−4578.

(22) Prieto, G.; Martínez, A.; Concepción, P.; Moreno-Tost, R. Cobalt Particle Size Effects in Fischer−Tropsch Synthesis: Structural and in Situ Spectroscopic Characterisation on Reverse Micelle-Synthesised Co/ITQ-2 Model Catalysts. *J. Catal.* **2009**, *266*, 129−144.

(23) Fischer, N.; van Steen, E.; Claeys, M. Structure Sensitivity of the Fischer−Tropsch Activity and Selectivity on Alumina Supported Cobalt Catalysts. *J. Catal.* **2013**, *299*, 67−80.

(24) Lögdberg, S.; Boutonnet, M.; Walmsley, J. C.; Järås, S.; Holmen, A.; Blekkan, E. A. Effect of Water on the Space-Time Yield of Different Supported Cobalt Catalysts during Fischer−Tropsch Synthesis. *Appl. Catal., A* **2011**, *393*, 109−121.

(25) Ralston, W. T.; Melaet, G.; Saephan, T.; Somorjai, G. A. Evidence of Structure Sensitivity in the Fischer−Tropsch Reaction on Model Cobalt Nanoparticles by Time-Resolved Chemical Transient Kinetics. *Angew. Chem., Int. Ed.* **2017**, *56*, 7415−7419.

(26) Melaet, G.; Lindeman, A. E.; Somorjai, G. A. Cobalt Particle Size Effects in the Fischer−Tropsch Synthesis and in the Hydrogenation of CO_2 Studied with Nanoparticle Model Catalysts on Silica. *Top. Catal.* **2014**, *57*, 500−507.

(27) Herranz, T.; Deng, X.; Cabot, A.; Guo, J.; Salmeron, M. Influence of the Cobalt Particle Size in the CO Hydrogenation Reaction Studied by In Situ X-Ray Absorption Spectroscopy. *J. Phys. Chem. B* **2009**, *113*, 10721−10727.

(28) Lee, Y.-J.; Park, J.-Y.; Jun, K.-W.; Wook Bae, J.; Prasad, P. S. S. Controlled Nanocrystal Deposition for Higher Degree of Reduction in Co/Al_2O_3 Catalyst. *Catal. Lett.* **2009**, *130*, 198−203.

(29) Park, J.-Y.; Lee, Y.-J.; Karandikar, P. R.; Jun, K.-W.; Ha, K.-S.; Park, H.-G. Fischer−Tropsch Catalysts Deposited with Size-Controlled Co_3O_4 Nanocrystals: Effect of Co Particle Size on Catalytic Activity and Stability. *Appl. Catal., A* **2012**, *411*−*412*, 15−23.

(30) Oukaci, R.; Singleton, A. H.; Goodwin, J. G. Comparison of Patented Co F−T Catalysts Using Fixed-Bed and Slurry Bubble Column Reactors. *Appl. Catal., A* **1999**, *186*, 129−144.

(31) Morales, F.; de Smit, E.; de Groot, F. M. F.; Visser, T.; Weckhuysen, B. M. Effects of Manganese Oxide Promoter on the CO and H_2 Adsorption Properties of Titania-Supported Cobalt Fischer−Tropsch Catalysts. *J. Catal.* **2007**, *246*, 91−99.

(32) Tauster, S. J.; Fung, S. C.; Garten, R. L. Strong Metal-Support Interactions. Group 8 Noble Metals Supported on TiO_2. *J. Am. Chem. Soc.* **1978**, *100*, 170−175.

(33) Tauster, S. J.; Fung, S. C.; Baker, R. T.; Horsley, J. A. Strong Interactions in Supported-Metal Catalysts. *Science* **1981**, *211*, 1121−1125.

(34) Eschemann, T. O.; de Jong, K. P. Deactivation Behavior of Co/TiO_2 Catalysts during Fischer−Tropsch Synthesis. *ACS Catal.* **2015**, *5*, 3181−3188.

(35) Hong, J.; Du, J.; Wang, B.; Zhang, Y.; Liu, C.; Xiong, H.; Sun, F.; Chen, S.; Li, J. Plasma-Assisted Preparation of Highly Dispersed Cobalt Catalysts for Enhanced Fischer−Tropsch Synthesis Performance. *ACS Catal.* **2018**, *8*, 6177−6185.

(36) Delgado, J. A.; Claver, C.; Castillón, S.; Curulla-Ferré, D.; Ordomsky, V. V.; Godard, C. Fischer−Tropsch Synthesis Catalysed

DOI: 10.1021/acscatal.8b03094
ACS Catal. 2018, 8, 10581−10589

by Small TiO_2 Supported Cobalt Nanoparticles Prepared by Sodium Borohydride Reduction. *Appl. Catal., A* **2016**, *513*, 39−46.
(37) Delgado, J. A.; Claver, C.; Castillón, S.; Curulla-Ferré, D.; Ordomsky, V. V.; Godard, C. Effect of Polymeric Stabilizers on Fischer−Tropsch Synthesis Catalyzed by Cobalt Nanoparticles Supported on TiO_2. *J. Mol. Catal. A: Chem.* **2016**, *417*, 43−52.
(38) Melaet, G.; Ralston, W. T.; Li, C.-S.; Alayoglu, S.; An, K.; Musselwhite, N.; Kalkan, B.; Somorjai, G. A. Evidence of Highly Active Cobalt Oxide Catalyst for the Fischer−Tropsch Synthesis and CO_2 Hydrogenation. *J. Am. Chem. Soc.* **2014**, *136*, 2260−2263.
(39) Iablokov, V.; Beaumont, S. K.; Alayoglu, S.; Pushkarev, V. V.; Specht, C.; Gao, J.; Alivisatos, A. P.; Kruse, N.; Somorjai, G. A. Size-Controlled Model Co Nanoparticle Catalysts for CO_2 Hydrogenation: Synthesis, Characterization, and Catalytic Reactions. *Nano Lett.* **2012**, *12*, 3091−3096.
(40) Casavola, M.; Hermannsdörfer, J.; de Jonge, N.; Dugulan, A. I.; de Jong, K. P. Fabrication of Fischer−Tropsch Catalysts by Deposition of Iron Nanocrystals on Carbon Nanotubes. *Adv. Funct. Mater.* **2015**, *25*, 5309−5319.
(41) Reuel, R. C.; Bartholomew, C. H. The Stoichiometries of H_2 and CO Adsorptions on Cobalt: Effects of Support and Preparation. *J. Catal.* **1984**, *85*, 63−77.
(42) Zacharaki, E.; Kalyva, M.; Fjellvåg, H.; Sjåstad, A. O. Burst Nucleation by Hot Injection for Size Controlled Synthesis of ε-Cobalt Nanoparticles. *Chem. Cent. J.* **2016**, *10*, 10.
(43) Wolf, M.; Fischer, N.; Claeys, M. Effectiveness of Catalyst Passivation Techniques Studied in Situ with a Magnetometer. *Catal. Today* **2016**, *275*, 135−140.
(44) Hernández Mejía, C.; van Deelen, T. W.; de Jong, K. P. Activity Enhancement of Cobalt Catalysts by Tuning Metal-Support Interactions. *Nat. Commun.* Accepted.
(45) Sadasivan, S.; Bellabarba, R. M.; Tooze, R. P. Size Dependent Reduction-Oxidation-Reduction Behaviour of Cobalt Oxide Nanocrystals. *Nanoscale* **2013**, *5*, 11139−11146.
(46) Wolf, M.; Kotzé, H.; Fischer, N.; Claeys, M. Size Dependent Stability of Cobalt Nanoparticles in High Conversion Fischer−Tropsch Environment. *Faraday Discuss.* **2017**, *197*, 243−268.
(47) van Steen, E.; Claeys, M.; Dry, M. E.; van de Loosdrecht, J.; Viljoen, E. L.; Visagie, J. L. Stability of Nanocrystals: Thermodynamic Analysis of Oxidation and Re-Reduction of Cobalt in Water/Hydrogen Mixtures. *J. Phys. Chem. B* **2005**, *109*, 3575−3577.
(48) Tsakoumis, N. E.; Walmsley, J. C.; Rønning, M.; van Beek, W.; Rytter, E.; Holmen, A. Evaluation of Reoxidation Thresholds for γ−Al_2O_3−Supported Cobalt Catalysts under Fischer−Tropsch Synthesis Conditions. *J. Am. Chem. Soc.* **2017**, *139*, 3706−3715.
(49) Prieto, G.; De Mello, M. I. S.; Concepción, P.; Murciano, R.; Pergher, S. B. C.; Martinez, A. Cobalt-Catalyzed Fischer−Tropsch Synthesis: Chemical Nature of the Oxide Support as a Performance Descriptor. *ACS Catal.* **2015**, *5*, 3323−3335.
(50) Yang, J.; Tveten, E. Z.; Chen, D.; Holmen, A. Understanding the Effect of Cobalt Particle Size on Fischer−Tropsch Synthesis: Surface Species and Mechanistic Studies by SSITKA and Kinetic Isotope Effect. *Langmuir* **2010**, *26*, 16558−16567.
(51) Kliewer, C. E.; Soled, S. L.; Kiss, G. Morphological Transformations during Fischer−Tropsch Synthesis on a Titania-Supported Cobalt Catalyst. *Catal. Today* **2018**, DOI: 10.1016/j.cattod.2018.05.021.
(52) Iglesia, E.; Soled, S. L.; Fiato, R. A. Fischer−Tropsch Synthesis on Cobalt and Ruthenium. Metal Dispersion and Support Effects on Reaction Rate and Selectivity. *J. Catal.* **1992**, *137*, 212−224.
(53) Iglesia, E. Design, Synthesis, and Use of Cobalt-Based Fischer−Tropsch Synthesis Catalysts. *Appl. Catal., A* **1997**, *161*, 59−78.
(54) Storsæter, S.; Borg, Ø.; Blekkan, E. A.; Holmen, A. Study of the Effect of Water on Fischer−Tropsch Synthesis over Supported Cobalt Catalysts. *J. Catal.* **2005**, *231*, 405−419.
(55) Munnik, P.; de Jongh, P. E.; de Jong, K. P. Control and Impact of the Nanoscale Distribution of Supported Cobalt Particles Used in Fischer−Tropsch Catalysis. *J. Am. Chem. Soc.* **2014**, *136*, 7333−7340.
(56) Eschemann, T. O.; Lamme, W. S.; Manchester, R. L.; Parmentier, T. E.; Cognigni, A.; Rønning, M.; de Jong, K. P. Effect of Support Surface Treatment on the Synthesis, Structure, and Performance of Co/CNT Fischer−Tropsch Catalysts. *J. Catal.* **2015**, *328*, 130−138.
(57) Campbell, C. T.; Mao, Z. Chemical Potential of Metal Atoms in Supported Nanoparticles: Dependence upon Particle Size and Support. *ACS Catal.* **2017**, *7*, 8460−8466.
(58) Munnik, P.; Velthoen, M. E. Z.; de Jongh, P. E.; De Jong, K. P.; Gommes, C. J. Nanoparticle Growth in Supported Nickel Catalysts during Methanation Reaction-Larger Is Better. *Angew. Chem., Int. Ed.* **2014**, *53*, 9493−9497.
(59) Ouyang, R.; Liu, J.-X.; Li, W.-X. Atomistic Theory of Ostwald Ripening and Disintegration of Supported Metal Particles under Reaction Conditions. *J. Am. Chem. Soc.* **2013**, *135*, 1760−1771.
(60) Wilson, J.; de Groot, C. P. M. Atomic-Scale Restructuring in High-Pressure Catalysis. *J. Phys. Chem.* **1995**, *99*, 7860−7866.
(61) Claeys, M.; Dry, M. E.; van Steen, E.; van Berge, P. J.; Booyens, S.; Crous, R.; Van Helden, P.; Labuschagne, J.; Moodley, D. J.; Saib, A. M. Impact of Process Conditions on the Sintering Behavior of an Alumina-Supported Cobalt Fischer−Tropsch Catalyst Studied with an in Situ Magnetometer. *ACS Catal.* **2015**, *5*, 841−852.
(62) Janse van Rensburg, W.; van Helden, P.; Moodley, D. J.; Claeys, M.; Petersen, M. A.; van Steen, E. Role of Transient Co-Subcarbonyls in Ostwald Ripening Sintering of Cobalt Supported on γ-Alumina Surfaces. *J. Phys. Chem. C* **2017**, *121*, 16739−16753.
(63) Jongsomjit, B.; Sakdamnuson, C.; Goodwin, J. G.; Praserthdam, P. Co-Support Compound Formation in Titania-Supported Cobalt Catalyst. *Catal. Lett.* **2004**, *94*, 209−215.
(64) Cats, K. H.; Andrews, J. C.; Stéphan, O.; March, K.; Karunakaran, C.; Meirer, F.; de Groot, F. M. F.; Weckhuysen, B. M. Active Phase Distribution Changes within a Catalyst Particle during Fischer−Tropsch Synthesis as Revealed by Multi-Scale Microscopy. *Catal. Sci. Technol.* **2016**, *6*, 4438−4449.
(65) Riva, R.; Miessner, H.; Vitali, R.; Del Piero, G. Metal−support Interaction in Co/SiO_2 and Co/TiO_2. *Appl. Catal., A* **2000**, *196*, 111−123.
(66) Wang, C.-B.; Cai, Y.; Wachs, I. E. Reaction-Induced Spreading of Metal Oxides onto Surfaces of Oxide Supports during Alcohol Oxidation: Phenomenon, Nature, and Mechanisms. *Langmuir* **1999**, *15*, 1223−1235.
(67) Kistamurthy, D.; Saib, A. M.; Moodley, D. J.; Niemantsverdriet, J. W.; Weststrate, C. J. Ostwald Ripening on a Planar Co/SiO_2 Catalyst Exposed to Model Fischer−Tropsch Synthesis Conditions. *J. Catal.* **2015**, *328*, 123−129.
(68) Hu, S.; Li, W.-X. Influence of Particle Size Distribution on Life Time and Thermal Stability of Ostwald Ripening of Supported Particles. *ChemCatChem* **2018**, *10*, 2900−2907.
(69) Wettergren, K.; Schweinberger, F. F.; Deiana, D.; Ridge, C. J.; Crampton, A. S.; Rötzer, M. D.; Hansen, T. W.; Zhdanov, V. P.; Heiz, U.; Langhammer, C. High Sintering Resistance of Size-Selected Platinum Cluster Catalysts by Suppressed Ostwald Ripening. *Nano Lett.* **2014**, *14*, 5803−5809.
(70) Zhang, S.; Cargnello, M.; Cai, W.; Murray, C. B.; Graham, G. W.; Pan, X. Revealing Particle Growth Mechanisms by Combining High-Surface-Area Catalysts Made with Monodisperse Particles and Electron Microscopy Conducted at Atmospheric Pressure. *J. Catal.* **2016**, *337*, 240−247.
(71) Xaba, B. M.; de Villiers, J. P. R. Sintering Behaviour of TiO_2-Supported Model Cobalt Fischer−Tropsch Catalysts under H_2 Reducing Conditions and Elevated Temperature. *Ind. Eng. Chem. Res.* **2016**, *55*, 9397−9407.

DOI: 10.1021/acscatal.8b03094
ACS Catal. 2018, 8, 10581−10589